Received 13 April 2021; revised 30 May 2021; accepted 20 June 2021. Date of publication 1 July 2021; date of current version 13 July 2021.

Digital Object Identifier 10.1109/OJCOMS.2021.3093106

Demand-Based Adaptive Multi-Beam Pattern and Footprint Planning for High Throughput GEO Satellite Systems

PUNEETH JUBBA HONNAIAH [1] (Graduate Student Member, IEEE), NICOLA MATURO [1] (Member, IEEE), SYMEON CHATZINOTAS [1] (Senior Member, IEEE), STEVEN KISSELEFF [1] (Member, IEEE), AND JENS KRAUSE [2]

[1] Interdisciplinary Centre for Security, Reliability and Trust (SnT), University of Luxembourg, 1511 Luxembourg City, Luxembourg

[2] RF Systems Development Department, SES S.A., 6815 Betzdorf, Luxemburg

CORRESPONDING AUTHOR: P. J. HONNAIAH (e-mail: puneeth.jubba-honnaiah@uni.lu)

This work was supported in part by the Luxembourg National Research Fund (FNR) under Industrial Fellowship Scheme with industrial partner SES S.A., project title "Resource Allocation and Interference Mitigation for demand based Capacity Adaptability in Satellite Communication System (REGAL)," under Grant FNR14147087, and in part by Luxembourg National Research Fund—Bridges Program, project title "Dynamic Beam Forming and In-Band Signalling for Next Generation Satellite Systems (DISBuS)."

ABSTRACT The current broadband coverage area requisites and the expected user demand is satisfied by the state of the art satellite industry by using multiple spot beams of high throughput satellites with fixed multi-beam pattern and footprint planning. However, in recent years, new mobile broadband users with dynamic traffic demand are requesting for services in remote geographical locations such as air (aeroplanes) and water (ships). Furthermore, the expected demand varies with time and geographical location of the users. Hence, a practical approach to meet such heterogeneous demand is to plan adaptive beams to the satellites equipped with beamforming capabilities. In this paper, we study the state of the art fixed multi-beam pattern and footprint plan and show its drawbacks to support the non-uniformly distributed user terminals and varying traffic demands. To end this, we propose an adaptive multi-beam pattern and footprint plan where we design spot beams with flexible size and position based on the spatial clustering of the users in order to increase the flexibility of the high throughput satellite system. Numerical simulations demonstrate the high system performance of the proposed methodology.

INDEX TERMS Multi-beam high throughput satellite systems, beam pattern, beam footprint, DVB-S2X, precoding.

I. INTRODUCTION

INTERNET broadband services have gained immense attention not only for business competitiveness but also for helping social inclusion. While most of the broadband demand in the urban regions are satisfied using terrestrial technologies, the broadband demand in the remote locations strongly relies on satellite broadband services [1]. Lately, the increase in the demand has made satellite providers switch from legacy single beam architecture to High Throughput Satellite (HTS) systems with multiple spot beams which reuse carrier bandwidth across several beams to satisfy the rising demand [2]. Since the launch of the first high-speed, all-digital communications satellite named Advanced Communications Technology Satellite (ACTS) by NASA, technologies such as Onboard Digital Processing (ODP) and Switching has been widely popular. More recently, the shape and position of satellite beams can be adjusted using Dynamic Beamforming Networks (DBN) to enhance frequency utilization efficiency through space-division multiplexing [3]. The radiation pattern of antenna arrays can be controlled using the beamforming technique, without physical movement of the antennas [4] and hence is key enabler for the adaptive beam pattern and footprint plan.

TABLE 1. Table of acronyms.

HTS	High Throughput Satellites
FMPF	Fixed Multi-beam Pattern and Footprint
AMPF	Adaptive Multi-beam Pattern and Footprint
DBN	Dynamic Beamforming Networks
ACTS	Advanced Communications Technology Satellite
ODP	Onboard Digital Processing
FSS	Fixed Satellite Sevices
QoS	Quality of service
AFR	Array-Fed Reflector
PFD	Flux Density
ESA	European Space Agency
WED	Weighted Euclidean Distance
DM	Distance Metric
PAM	Partitioning Around Medoids
CLARA	ClusteringLARge Applications
SEDAC	SocioEconomic Data and Applications Center
CDF	Cumulative Distribution Function
NCD	Normalized Capacity Deviation

A. LITERATURE REVIEW

There exist a dearth of efficient beam footprint plans in literature. The authors of [5] have made an early contribution in planing the beam layout of a reflector multi-beam antenna with overlapping beams. The authors of [6] compare the conventional contoured beam antennas with multi-beam antenna and propose fixed beam diameters for a specified number of beams to ensure global coverage using overlapping spot beams with a hexagonal grid layout. Furthermore, the authors of [7]–[9] discuss the antenna requirements to plan a good beam pattern for fixed beam footprint plans. Hence, all the early works consider only the geometric feasibility of the spot beams in the beam pattern and footprint plan, and focus on having hexagonal beams of equal size and ensure global coverage. Therefore, the coverage region and the offered throughput remains same for all of the multiple spot beams irrespective of the traffic demand.

However, much recent works have focused on adaptive plans to accommodate fluctuations in traffic demand. The authors of [10] discuss the global resource management for dynamic beam steering due to changes in QoS requirements and channel conditions of users. The authors of [11] optimize beam-directivity and transmit-power according to traffic demand to improve the overall system throughput. The authors of [12] adapt satellite's transmitting antenna boresight to maximize signal to noise power ratio (SNR) of satellite ground station and minimize interference to terrestrial networks. The authors of [13] propose an optimization tool to jointly optimize the number of beams, beam width, power and bandwidth allocation in order to match the provided data rate to the predicted traffic demand but do not optimize the beam positions and beam shape. The authors of [14] propose a mathematical model to derive multi-spot beam arrangements and discuss the relationship between the placement of a multi-spot beam and user throughput. They study only the effect of geographic distances between spot beams in the same frequency band and the geographic distances between adjacent spot beams in different frequency bands on the overall system throughput but do not implement adaptability in terms of flexible beam size and beam position in beam plan. To the best of our knowledge, none of the authors have considered the mobility aspects of the non-uniformly distributed users and dynamically changing beam demand during the beam pattern and footprint planning. Also, unlike the recent works, the proposed network planning is not a static process but a dynamic one that has to be repeated multiple times during a day. Furthermore, in all the previous works some beams are under-used while others are too crowded and hence is only a sub optimal solution.

B. CONTRIBUTION

The contribution of the paper is as follows.

1) We propose a novel Adaptive Multi-beam Pattern and Footprint (AMPF) plan that achieve even traffic load distribution across all the beams in the HTS system that simplifies the radio resource management, payload allocation and frequency allocation. To achieve such plan, in this work, we not only consider spatiotemporally varying traffic demand but also the distributed and non-uniform mobile geographic locations of the users.
2) We propose a novel method for the planning of the multi-beam pattern based on geographical clustering (weighted K-means clustering) of the users, which is optimally matched to the heterogeneous demand distribution within the field of view of the satellite. Using the proposed method it is possible to reduce the variations of the traffic load among the beams, which leads to better traffic matching.
3) To ensure a required coverage region, we use Voronoi Tessellation to plan irregular non-hexagonal convex Voronoi polygons as beam regions. Such an approach is relatively new in beam pattern and footprint plan.
4) Contrary to the related works, in AMPF plan, we propose elliptical beams which add in one more degree of freedom for beam footprint plan.
5) Lastly, unlike the previous works, to plan practical and meaningful antenna patterns, we consider the design parameters of the beam pattern and footprint parameters in the angular domain as seen from the satellite. This is because the satellite beam is defined with parameters that are in fact angles centred at the satellite. Hence, the gain pattern of the antenna which is on-board the satellite is naturally described in the satellite angular domain as ellipses. However, when these elliptical gain patterns are projected on the surface of the Earth, they undergo distortion in both beam shape (ellipses taking the shape of convex polygons) and power flux density. Hence, performing user clustering and beam planning on the satellite angular domain prevents the errors introduced by such distortions.

The rest of the paper is organised as follows. In Section II, the system model employing Multi-beam High Throughput

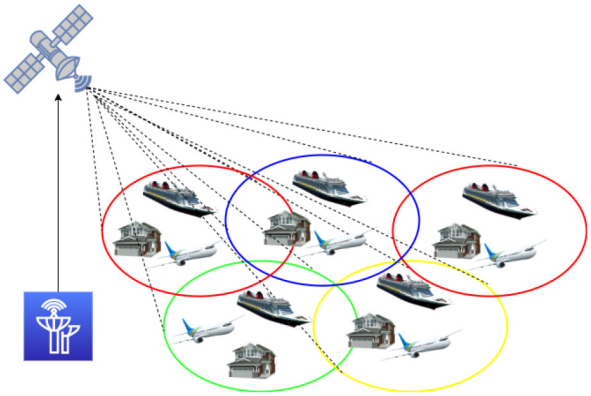

FIGURE 1. High throughput Multi-beam Satellite System architecture using four colour scheme.

Satellite channel, beam footprint and pattern is described. In Section III, the problem statement is defined. A novel method for the beam pattern footprint plan is explained in Section IV. Section V provides the simulation results, and Section VI concludes the paper.

Notation: We use upper-case and lower-case bold-faced letters to denote matrices and vectors, respectively. $\circ$ denotes the element-wise Hadamard operations, $(\cdot)^T$ denotes the transpose of $(\cdot)$. $\|.\|$ depicts the Euclidean norm, $\subseteq$ denotes subset and $P(.)$ denotes power set. If $\mathfrak{S}$ is a set, then $|\mathfrak{S}|$ denotes cardinality of set $\mathfrak{S}$ and if $\mathfrak{M}$ is a matrix, then $|\mathfrak{M}|$ denotes determinant of matrix $\mathfrak{M}$.

II. SYSTEM MODEL

A. MULTI-BEAM SATELLITE SYSTEM

We consider a Multi-beam Satellite system as shown in Figure 1 that employs multiple spot beams to provide the required coverage. Non-uniform and distributed broadband users including Fixed Satellite Services (FSS) users, aeronautical users and maritime users are considered. Furthermore, to reduce the interference at the beam edges, the four colours frequency reuse scheme [16] is employed such that every beam is allocated a different carrier frequency or a different polarization to that of its neighbor.

The space-segment consist of a programmable payload GEO satellite with Array-Fed Reflector (AFR) antennas with beamforming capabilities that can alter the beam size and beam positions by digital signal processing.

The Gateway is a ground station and is connected to the Internet backbone network. We assume that the optimization is done in the ground station. Also, we assume that the traffic demand does not change very aggressively over time due to the user multiplexing effect.

B. BEAM FOOTPRINT AND BEAM PATTERN

The beam footprint of a Multi-beam satellite system shows the dispersion of multiple beams with defined beam widths across the ground area of its coverage. In this work, we consider elliptical beams generated in the satellite angular domain. This adds in one more degree of freedom to optimize the beam footprints. Nevertheless, the projection of these ellipses on the surface of the Earth will result in non-elliptical polygonal beams whose geodetic shape on the surface of the Earth expressed using Earth's latitude and Earth's longitude is dependent on the curvature of the Earth [15].

A beam pattern represents the magnitude of the electric or magnetic field, as a function of the angular space. The beam centre which defines the beam position is where the antenna gain of the beam is maximum. The beam widths that define the beam shape are the locations corresponding to the 3dB reduction of the antenna gain compared to the beam centre. A beam pattern plan involves prudently choosing multiple metrics such as number of beams, beam centre and beam widths of all the beams in a Multi-beam satellite system.

The authors of [16] and [17] approximate the beam contour using Bessel function for beam gain computation. However, as we consider the beam shape to be elliptical in the angular domain of the satellite, we approximate the beam contour to be a two-dimensional Gaussian function. Figure 2 shows the heat map corresponding to the Power Flux Density (PFD) for a single beam. Every elliptical beam corresponds to a specific value of beam widths $\delta\theta$ and $\delta\phi$ (defined by semi-major axis and semi-minor axis of the elliptical beam), beam centre, C (The point of intersection of semi-minor and semi-major axis) and the beam orientation or the tilt angle, φ.

The system capacity can be increased by increasing the number of beams in the forward link of the multi-beam satellite system. However, increasing the number of beams will increase the number of amplifiers in the space segment and this will increase both the manufacturing cost and the launch cost for the satellite operators. In our design, we consider 71 transmission beams in the forward link and do not optimize over the number of beams. The 71 beams constraint is applied to have a fair comparison with the benchmark FMPF reference beam pattern provided by European Space Agency (ESA) [18], [19]. Furthermore, the number of beams corresponds to the number of information streams that can be processed in parallel by the satellite payload. Switching off beams and thus info streams would require additional configuration changes on the payload.

C. MULTI-BEAM SATELLITE CHANNEL

We consider an HTS Multi-beam Satellite system with N broadband users and K beams. The received signal y_n at the user u_n in the k^{th} beam is as expressed as,

$$y_n = \mathbf{h}_n^T \mathbf{s} + \mathfrak{N}_n, \tag{1}$$

where $\mathbf{h}_n \in \mathbb{C}^{K\times 1}$ is the CSI vector corresponding to this particular user. $\mathbf{s} \in \mathbb{C}^{K\times 1}$ represents the transmitted signal vector. $\mathfrak{N}_n$ is a random variable distributed as $\mathcal{CN}(0, \sigma^2)$, modelling the zero-mean Additive White Gaussian Noise (AWGN) measured at the u_n's receiving antenna.

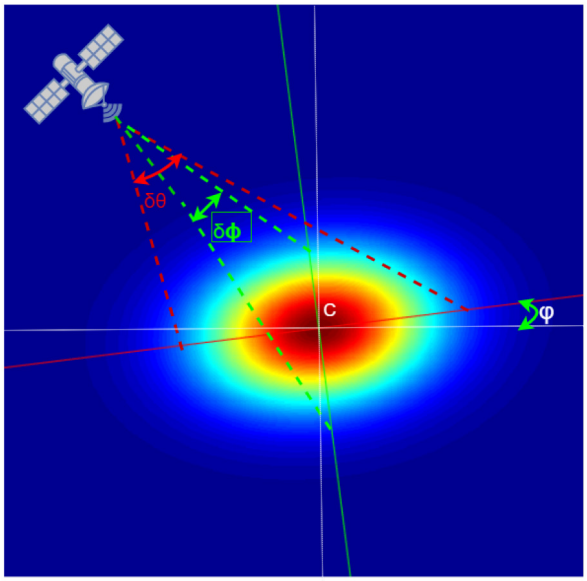

FIGURE 2. Two-dimensional Gaussian function approximation to define the beam pattern.

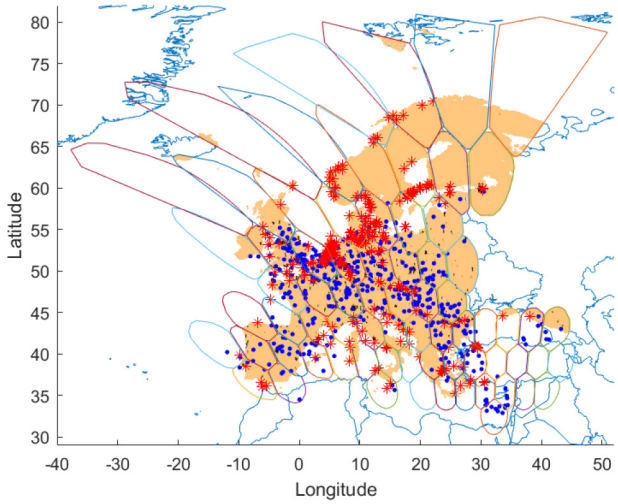

FIGURE 3. Benchmark FMPF plan beam footprint over Europe using 71 Fixed Beams showing flight user locations in blue, ship user locations in red and FSS user locations in beige.

By rearranging all the users' received signals in a vector $\mathbf{y} = [y_1 \dots y_N]^T \in \mathbb{C}^{K\times 1}$, we can rewrite the above model as,

$$\mathbf{y} = \mathbf{H}\ \mathbf{s} + \mathfrak{N}, \tag{2}$$

where $\mathbf{H} = [\mathbf{h}_1 \dots \mathbf{h}_N]^T$ represents the system channel matrix, which is determined by the satellite antenna gain, the path loss, the received antenna gain and the noise power. More precisely, the (n, k)th component of $\mathbf{H}$ is given by,

$$[\mathbf{h}]_{n,k} = \frac{\sqrt{G_R n G_k n}}{\left(4\pi \frac{\mathfrak{D}_{nk}}{\lambda}\right)}, \tag{3}$$

where G_{Rn} is the receiver antenna gain (that mainly depends on the receiving antenna aperture) and G_{kn} are the gains defined by the multibeam satellite radiation pattern and user locations. $\mathfrak{D}_{nk}$ is the distance between the satellite transmit antenna k and the nth user's receiving antenna. Usually, due to the long propagation distance, $\mathfrak{D}_{nk} \approx \mathfrak{D}_n$. Finally, λ is the wavelength of transmission.

III. PROBLEM STATEMENT

The benchmark FMPF plan system comprises of a fixed number of beams with predetermined beam shape obtained by 71-beam GEO 0E satellite operating at the Ka exclusive band 19.7 to 20.2 GHz [20]–[22] is as shown in Figure 3. The fixed plan provides coverage to the Europe region using 71 beams. However, broadband users across Europe are not uniformly distributed and the broadband traffic demand for an FSS user defers from a maritime user. Also, aeronautical and maritime users are mobile users and their positions vary with time. In benchmark FMPF plan, as the position and size of the beams are fixed, the offered throughput remains relatively similar across all the beams irrespective of change in the number of users in the beam and beam demand. Therefore, such rigid plans will fail to distribute broadband traffic demand across all the beams evenly and result in either under-use the offered throughput (beam capacity is unused) or overload the beam (beam demand is unmet).

Therefore, to plan adaptive beams for mobile users with variable demand, we first need to find the best partition of all the users into sets of adjacent users in an euclidean sense such that total system demand is evenly distributed among all the sets and then, plan a beam which is suitable to serve each user set.

Similar set partitioning problems but for a different application is discussed in [23] and is an optimization form of exact cover. To solve set partitioning problems, we find the best disjoint cover within some collection $\mathcal{S} = \{\mathcal{S}^1, \mathcal{S}^2 \cdots \mathcal{S}^K\} \subseteq \mathcal{P}(\mathcal{N})$, where $\mathcal{N}$ is the universal set containing all the broadband users in the system and $\mathcal{P}(\mathcal{N})$ is the power set of $\mathcal{N}$. We define the convex hull of any set $\mathcal{S}^k$ as,

$$\mathcal{H}^k = \sum_{n\in\mathcal{S}^k} \lambda_n \mathbf{x}_n : \lambda_n \geq 0 \quad \forall n, \quad \sum_{n\in\mathcal{S}^k} \lambda_n = 1 \tag{4}$$

where $\mathbf{x}_n$ as the 2D coordinate vector of a broadband user n.

We define d_n as the traffic demand and $D_k = \sum_{n\in\mathcal{S}^k} d_n$ as the beam demand that corresponds to the sum of the demand of all the users belonging to the beam k.

The objective function is fair distribution of the system demand across all the beams and is defined as,

$$\max_{\mathcal{S}} \ \frac{\left(\sum_{k=1}^{K} D_k\right)^2}{K\sum_{k=1}^{K} D_k^2}; \tag{5a}$$

$$\text{Subject to } \bigcup_{k=1}^{K} \mathcal{S}^k = \mathcal{N}, \tag{5b}$$

$$\mathcal{S}^i \cap \mathcal{S}^j = \emptyset, \forall i \neq j \tag{5c}$$

$$\mathcal{S}^i \neq \emptyset, \forall i, \tag{5d}$$

$$\mathcal{H}^i \cap \mathcal{H}^j = \emptyset, \forall i \neq j, \tag{5e}$$

where the first constraint in (5b) ensures that all the users are under the coverage region. The second constraint in (5c) assures that any user will be served by only one beam. The third constraint mentioned in (5d) ensures that the beams have at least one user and to avoid planning beams with zero demand. The last constraint in (5e) guarantees that each partitioned set is a convex set and assures that the convex hulls' of partitioned sets do not overlap within the 2D Euclidean space. In this approach, the feasible solutions cover the universal set $\mathcal{N}$ rather than any of its subsets and hence is a restricted setting of set partitioning.

However, set partitioning problems are non-deterministic polynomial acceptable problems that are NP-hard and are at least as hard as the hardest problems in NP [24]. Therefore, solving the set partition problem by optimizing for best disjoint cover using classical optimization techniques is either cumbersome [25] or does not guarantee a global minimum [26].

Alternatively, partitioning problems can also be solved using clustering methods [27]. But, the optimizing problem in clustering methods is also NP-hard. However, clustering methods are iterative and offer probabilistic guarantees [28]. To define the problem using clustering approach, we consider metric spaces where we endow universe $\mathcal{N}$ with a metric space $(\mathcal{X}, r)$ such that $\mathcal{N} \subseteq \mathcal{X}$, where $\mathcal{X}$ is a set of all points in a 2D Euclidean space and r is a distance metric on $\mathcal{X}$. Then to obtain the cluster sets $\{\mathcal{T}^1, \mathcal{T}^2 \dots \mathcal{T}^K\}$ that are optimized for even demand distribution, we can define the partitioning problem using clustering by,

$$\underset{\{\mathcal{T}^1, \mathcal{T}^2 \dots \mathcal{T}^K\}}{\text{minimize}} \sum_{k=1}^{K} \sum_{n \in \mathcal{T}^k} r(\mathbf{x}_n, \boldsymbol{c}_{\mathcal{T}^k}) \left(\frac{\sum_{n \in \mathcal{T}^k} (d_n)}{\sum_{n=1}^{N} (d_n)} \right); \tag{6a}$$

$$\text{Subject to} \bigcup_{k=1}^{K} \mathcal{T}^k = \mathcal{N}, \tag{6b}$$

$$\mathcal{T}^i \cap \mathcal{T}^j = \emptyset, \forall i \neq j, \tag{6c}$$

$$\mathcal{T}^i \neq \emptyset, \forall i, \tag{6d}$$

$$\boldsymbol{c}_{\mathcal{T}^k} = \frac{1}{\sum_{n \in \mathcal{T}^k} d_n} \sum_{n \in \mathcal{T}^k} d_n \mathbf{x}_n. \tag{6e}$$

The objective function is the weighted distance of each cluster member from the cluster center, where $r(\mathbf{x}_n, \boldsymbol{c}_{\mathcal{T}^k}) = ((\mathbf{x}_n - \boldsymbol{c}_{\mathcal{T}^k})(\mathbf{x}_n - \boldsymbol{c}_{\mathcal{T}^k})')$ is the euclidean distance between any user n and the cluster center $\boldsymbol{c}_{\mathcal{T}^k}$. Weights are added to distribute the demand evenly among all the beams and are defined as the ratio of beam demand $(\sum_{n \in \mathcal{T}^k} d_n)$ to the system demand $(\sum_{n=1}^{N} d_n)$.

In the constraint (6e), $\boldsymbol{c}_{\mathcal{T}^k}$ is two element vector in the 2D Euclidean space representing the weighted cluster centroid of the cluster k. The clustered sets $\{\mathcal{T}^1, \mathcal{T}^2 \dots \mathcal{T}^K\}$ are by default convex sets and satisfies the constraint in (5e) and hence is not included in the clustering problem. It should be noted that even though the two problems are not equivalent, the clustering approach follows a similar rationale and provides easier structure.

Furthermore, the convex hulls $\{\mathcal{H}^1, \mathcal{H}^1 \dots \mathcal{H}^K\}$ encompassing the clusters $\{\mathcal{T}^1, \mathcal{T}^2 \dots \mathcal{T}^K\}$ are convex polygons in the 2D Euclidean space. Therefore, we have an additional problem on how to translate the vertex vectors of the convex polygon into simple beam shape that can be used as a template by the antenna and beamforming network designers. Henceforth, we propose to approximate convex polygons into ellipses. Early works [29], [30] in literature addresses the mathematical problem of approximating a convex polygon into an ellipse. However, in this work, we use an approach similar to [31] for its simplicity. Accordingly, if (x, y) represents vertex variables of the convex hull $\mathcal{H}^k$ in 2D Euclidean space, then any general bivariate quadratic curve which can be expressed as,

$$ax^2 + 2bxy + cy^2 + 2dx + 2fy + g = 0, \tag{7}$$

should satisfy the Equations,

$$\Delta = \begin{vmatrix} a & b & d \\ b & c & f \\ d & f & g \end{vmatrix} \neq 0, \tag{8a}$$

$$J = \begin{vmatrix} a & b \\ b & c \end{vmatrix} > 0, \tag{8b}$$

$$\frac{\Delta}{a + c} < 0, \tag{8c}$$

to be represented as an ellipse $(\mathcal{E}^k)$ for which we need to find the best parameters for a, b, c, d, f, g in the Least Square sense [31].

The ellipses $\{\mathcal{E}^1, \mathcal{E}^1 \cdots \mathcal{E}^K\}$ represents K proposed beam footprints. The center $(\boldsymbol{c}_k)$ of the ellipse $(\mathcal{E}^k)$ represents the position of beam k in 2D Euclidean space. The semi-major and semi-minor axis $(\delta\theta_k, \delta\phi_k)$ along with the rotation angle φ_k of the ellipse $(\mathcal{E}^k)$ represents the shape of the beam k.

IV. PROPOSED SOLUTION

In the proposed AMPF plan, we first obtain cluster sets that evenly distributes the traffic throughput demand across all the beams. Later we approximate the convex hull of the cluster sets to ellipse by choosing beam positions $(\boldsymbol{c}_k)$, beam size $(\delta\theta_k, \delta\phi_k)$ and beam shape (φ_k) of all the K beams. In this section, we discuss the steps involved in achieving such a plan.

1) Firstly, to generate physically meaningful antenna patterns and to avoid the distortions introduced due to the curvature of the Earth, we transform the geographical coordinates of the user locations to the coordinates of the satellite angular domain.
2) Then, based on the location and broadband traffic demand of the users in the satellite angular domain, the broadband users are grouped into K clusters using weighted k-means clustering. The users in the same cluster will represent all the users under a beam.

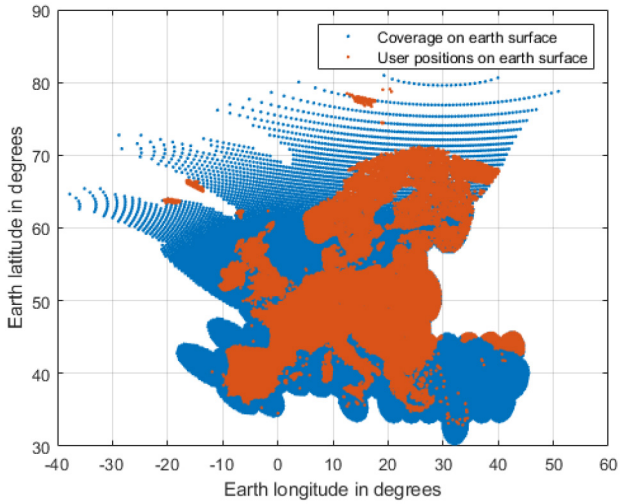

FIGURE 4. Sampled coverage area of the benchmark FMPF beams (shown in blue) and the user positions (shown in red) on the surface of the Earth.

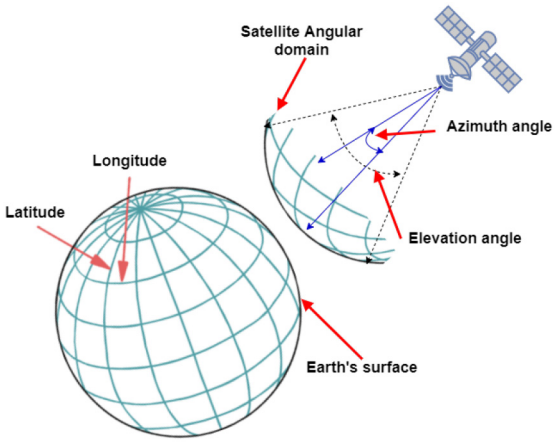

FIGURE 5. Difference between Earth's latitude-longitude domain and satellite angular domain. Latitude, longitude, elevation and azimuth angles are in degrees.

3) Later, to ensure full coverage, we use Voronoi Tessellation and define the beam borders.
4) However, the beam shapes generated using Voronoi Tessellation are irregular polygons. Hence, considering the mathematical tractability and for topological packing, we approximate the Voronoi Polygons by ellipses. Now, the centre of the ellipses ($\boldsymbol{c}_k$) will define the K beam positions, the semi-major and semi-minor axis of the ellipses ($\delta\theta_k$, $\delta\phi_k$) will define the boundary of the beams and angle of rotation of ellipses (φ_k) will define the shape of the proposed beams.
5) The proposed beams in satellite angular domain are now projected back on the surface of the Earth for visualization.
6) Furthermore, to measure the performance of the proposed plan with the benchmark FMPF plan, we fit a 2D Gaussian elliptical function on the approximated ellipse and perform link budget calculations.

A. DOMAIN TRANSFORMATION

The sampled coverage area of the benchmark FMPF beams and the user positions on the surface of the Earth obtained using [32] are expressed as geodetic positions using latitude and longitude, as shown in Figure 4. Figure 5 shows the relation between the latitude/longitude on the Earth's surface and azimuth/elevation on the satellite angular domain. In the spherical coordinate system, considering the centre of the Earth as origin, we use a spherical-ordered-triple (R_e radius-of-the-Earth (6,871,000 meters), Latitude (angle in degrees), Longitude (angle in degrees)) to describe the geodetic position of any user on the surface of the Earth. In the Cartesian coordinate system, the location of the user on the surface of the Earth is described using a Cartesian-ordered-triple in which each coordinate represents a distance.

We first convert the user position (Lat_U/Lon_U) from the spherical coordinate system to the Cartesian coordinate system expressed as Cartesian-ordered-triples ($X_{U,E}, Y_{U,E}, Z_{U,E}$) [33] using,

$$2X_{U,E} = R_e \times \cos(Lat_U) \times \cos(Lon_U), \tag{9a}$$
$$Y_{U,E} = R_e \times \cos(Lat_U) \times \sin(Lon_U), \tag{9b}$$
$$Z_{U,E} = R_e \times \sin(Lat_U). \tag{9c}$$

Similarly, we also convert the satellite position from the spherical coordinate system (Lat_S/Lon_S) to the Cartesian coordinate system ($X_{S,E}, Y_{S,E}, Z_{S,E}$). For such conversion, we consider a geostationary satellite with no tilt that orbits directly above the Earth's equator at the 0-degrees latitude and 0-degree longitude at an elevation of 35,786,000 meters. Then using user and satellite Cartesian-ordered-triples we estimate the position of the user considering the satellite as the origin using,

$$2X_{U,S} = X_{U,E} - X_{S,E}, \tag{10a}$$
$$Y_{U,S} = Y_{U,E} - Y_{S,E}, \tag{10b}$$
$$Z_{U,S} = Z_{U,E} - Z_{S,E}. \tag{10c}$$

Finally, we convert the user position from the Cartesian coordinate system to the spherical coordinate system [33] to get the user position in satellite angular domain using,

$$azimuth_U = \tan^{-1}\frac{Y_{U,S}}{X_{U,S}}, \tag{11a}$$
$$elevation_U = \tan^{-1}\frac{Z_{U,S}}{\sqrt{\left(X_{U,S}\right)^2 + \left(Y_{U,S}\right)^2}}. \tag{11b}$$

The geodetic positions are converted into the angular domain of the satellite and expressed in azimuth and elevation angles as shown in Figure 6.

B. CLUSTERING OF DISTRIBUTED USERS

Distributing the total broadband traffic demand across all the antenna beams evenly is not a straightforward solution because of the uneven geographic distribution of the broadband users and the geometric shape limitations of the antenna

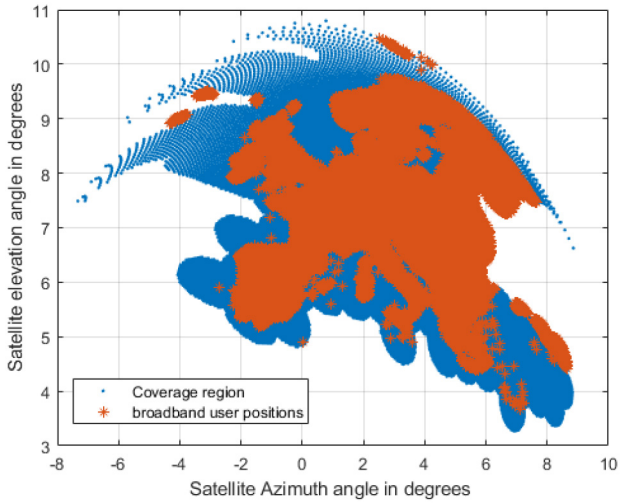

FIGURE 6. Sampled coverage area of the benchmark FMPF beams (shown in blue) and the user positions (shown in red) in satellite angular domain.

beam footprint. Hence, we use Cluster Analysis or Clustering to group traffic users into clusters and serve them under a beam [34]. There exist a plethora of literature [35] on clustering methods with application in computer vision and pattern recognition. The use of such clustering methods based on partition for beam pattern and footprint plan in Multi-beam satellite systems, which we propose in this paper, is a novel approach.

In Data Mining [36], Clustering is used to categorize the sample data into groups or clusters such that the objects in the same cluster are more related to each other than to the objects in different clusters. Using a similar approach, we considered the geographical locations and traffic demand of N broadband users as the sample data and assigned them to K clusters with each cluster to be converted to a beam in a later stage. We use the same number K for the number of clusters and beams, since each beam will serve one cluster. We have analysed various clustering algorithms such as k-means, k-medoids, Partitioning Around Medoids (PAM) and Clustering LARge Applications (CLARA) [37].

As all the above mentioned clustering methods assign each observation from the observation set to different cluster sets by minimizing the squared Euclidean distance from the data point to the mean or median location of its assigned cluster, they could be used to partition the N broadband users into K number of clusters $\{\mathcal{T}^1, \mathcal{T}^2 \ldots \mathcal{T}^K\}$ with $\{\boldsymbol{c}_{\mathcal{T}^1}, \boldsymbol{c}_{\mathcal{T}^2} \ldots \boldsymbol{c}_{\mathcal{T}^K}\}$ as cluster centres. However, among the various known clustering methods, we decided to employ weighted k-means clustering using iterative Lloyd's algorithm [38] approach. Lloyd's algorithm is known as a centroid tessellation, which is beneficial for the beam design, since the beam center is likely to point in the direction of the dominant group of users. Hence, the demand can be better satisfied. The steps of Lloyd's Iteration Partition Clustering is shown in Algorithm .

The initial K cluster centres in Step-1 of the Algorithm are chosen as cluster seeds using the k-means++ algorithm [39] for faster computation which converges better than random seeding. In Step-2, the distance matrix ($\mathfrak{R}_{K\times N}$) is computed using the Distance Metric (DM) between all the users and the cluster centres. Then using the distance matrix $\mathfrak{R}_{K\times N}$, the users are grouped into clusters to their nearest cluster centre. The Distance Metric used to compute the distances in the distance matrix $\mathfrak{R}_{K\times N}$ are a Weighted Euclidean Distances (WED) and is expressed as,

$$\mathrm{WED}_{(\mathbf{x}_\mathrm{n}, \boldsymbol{c}_{\mathcal{T}^\mathrm{k}})} = \left(\left(\mathbf{x}_\mathrm{n} - \boldsymbol{c}_{\mathcal{T}^\mathrm{k}}\right)\left(\mathbf{x}_\mathrm{n} - \boldsymbol{c}_{\mathcal{T}^\mathrm{k}}\right)'\right)\left(\frac{\sum_{\mathrm{n}\in\mathcal{T}^\mathrm{k}}(\mathrm{d_n})}{\sum_{\mathrm{n}=1}^{\mathrm{N}}(\mathrm{d_n})}\right), \tag{12}$$

where d_n is the broadband traffic demand of any user n. The WED will ensure that the clustering is based not only on their geographical location but also on their broadband traffic demand. In Step 4, a weighted version of the mean user position is computed as a cluster centre $\boldsymbol{c}_{\mathcal{T}^k}$ using,

$$\boldsymbol{c}_{\mathcal{T}^k} = \frac{1}{\sum_{n\in\mathcal{T}^k} d_n} \sum_{n\in\mathcal{T}^k} d_n \mathbf{x}_n. \tag{13}$$

The Step-2 to Step-4 are repeated in Lloyd's iteration fashion for better clustering. The algorithm stops either when the cluster assignments do not change or when the maximum number of iterations are reached. We assume the maximum number of iterations to be 500 is usually sufficient for a good convergence. Upon the termination of the algorithm, all the broadband users will be grouped into K clusters $\{\mathcal{T}^1, \mathcal{T}^2 \ldots \mathcal{T}^K\}$.

C. VORONOI TESSELLATION

As clustering is based on current broadband user positions, all broadband users in the cluster will be covered by the cluster contour. So, we can define the boundary of the beam around the clustered users in the satellite angular domain. But, by defining the cluster boundary as beam boundary, we may create uncovered regions between beams where there is no coverage. Also, as the geographical locations of the maritime and the aeronautical broadband users change, it is necessary to plan beam boundaries such that no area remains uncovered. Also, for a fair comparison with the benchmark FMPF plan, we would like to guarantee the coverage in all areas, where the coverage is provided by the benchmark design method. For this we employ Voronoi Tessellation [40] in order to define the beam boundaries.

The definition of the Voronoi Tessellation [41] can be expressed as,

$$\begin{aligned} \mathrm{dom}(\mathcal{M}, \mathcal{N}) &= \{x \in \mathcal{X} : r(x, \mathcal{M}) \leq r(x, \mathcal{N})\} \\ \text{where, } r(x, \mathcal{N}) &= \inf\{r(x, n) : n \in \mathcal{N}\} \end{aligned} \tag{14}$$

where if $(\mathcal{X}, r)$ is a metric space where $\mathcal{X}$ is a set of all points in a 2D Euclidean space and r is a distance metric on $\mathcal{X}$, then given two nonempty sets $\mathcal{M}, \mathcal{N} \subseteq \mathcal{X}$, the dominance

Algorithm 1 Loyd's Iteration Partition Clustering Algorithm

procedure CLUSTERING $(K, X, d, D_{K\times N}, C_s, DM, M)$ ▷
K= Total number of beams,
$X = \{\boldsymbol{x}_1, \boldsymbol{x}_2 ... \boldsymbol{x}_N\}$ = Broadband user set,
$d = \{d_1, d_2 ... d_N\}$ = User demand in Mbps,
$C_s = \{\boldsymbol{c}_{\mathcal{T}^1}, \boldsymbol{c}_{\mathcal{T}^2} ... \boldsymbol{c}_{\mathcal{T}^k}\}$ = Initial seeds for cluster centres,
DM = Distance Metric,
$\mathfrak{R}_{K\times N}$ = distance matrix,
M = Maximum number of iterations

[Step 1] Choose cluster centres $\{\boldsymbol{c}_{\mathcal{T}^1}, \boldsymbol{c}_{\mathcal{T}^2} ... c_{\mathcal{T}^k}\}$ defined by C_s selected as per $k-means++$ Algorithm.

while (Cluster assignments do not change) OR (M is not reached) **do**

[Step 2] Compute distance $\mathfrak{R}_{K\times N}$ between each of $\{\boldsymbol{c}_{\mathcal{T}^1}, \boldsymbol{c}_{\mathcal{T}^2} ... \boldsymbol{c}_{\mathcal{T}^k}\}$ and all of $\{\boldsymbol{x}_1, \boldsymbol{x}_2 ... \boldsymbol{x}_N\}$ using DM shown in (12).

[Step 3] Assign $\{\boldsymbol{x}_1, \boldsymbol{x}_2 ... \boldsymbol{x}_N\}$ users to K clusters $\{\mathcal{T}^1, \mathcal{T}^2 ... \mathcal{T}^K\}$ based on the minimum distance between the users and cluster centre using $\mathfrak{R}_{K\times N}$.

[Step 4] Compute new cluster centres $\{\boldsymbol{c}_{\mathcal{T}^1}, \boldsymbol{c}_{\mathcal{T}^2} ... \boldsymbol{c}_{\mathcal{T}^k}\}$ by using (13).

end While
end procedure

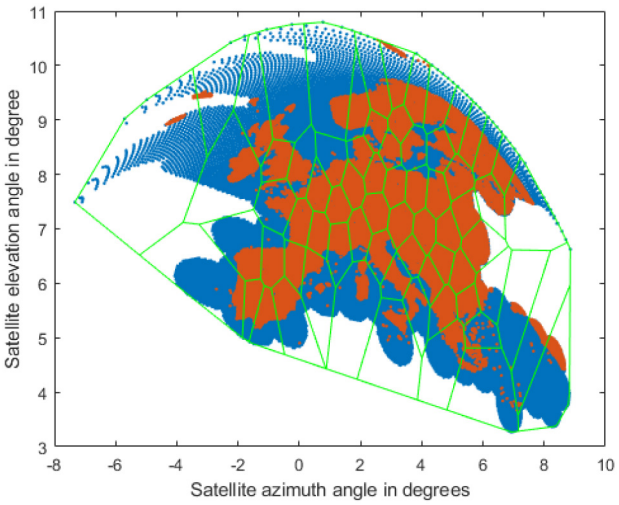

FIGURE 7. Beam boundaries (shown using green convex polygons) defined by Voronoi Tessellations in satellite angular domain. Sampled coverage area is shown in blue and the user positions are shown in red.

region $dom(\mathcal{M}, \mathcal{N})$ of $\mathcal{M}$ with respect to $\mathcal{N}$ is the set of all $x \in \mathcal{X}$ which are closer to $\mathcal{M}$ than to $\mathcal{N}$. In other words, for any point in a set of co-planar points, a boundary could be derived encompassing it such that the region inside the boundary includes all points nearer to it than to any other point in the set. Furthermore, such boundary defines one Voronoi polygon. The collection of all Voronoi polygons for every point in the set is called a Voronoi Tessellation.

We consider the cluster centres $\{\boldsymbol{c}_{\mathcal{T}^1}, \boldsymbol{c}_{\mathcal{T}^2} \dots \boldsymbol{c}_{\mathcal{T}^K}\}$ obtained by weighted k-means user clustering in Euclidean plane. Any centre $\boldsymbol{c}_{\mathcal{T}^k}$ is simply a point in the Euclidean plane, and its corresponding Voronoi cell V_u consists of every point in the Euclidean plane whose Euclidean distance to $\boldsymbol{c}_{\mathcal{T}^u}$ is less than or equal to its Euclidean distance to any other centre $\boldsymbol{c}_{\mathcal{T}^{v\neq u}}$. Each such Voronoi cell is obtained from the intersection of geometric half-spaces, and hence it is a convex polygon. The collection of such convex Voronoi polygons distributed in the satellite coverage region of Europe in the angular domain is shown in Figure 7. We approximate the boundary of Voronoi polygons as beam contour and the geographic centres $\{\boldsymbol{c}'_1, \boldsymbol{c}'_2 \dots \boldsymbol{c}'_K\}$ of Voronoi polygons as beam centres. However, from the antenna pattern perspective, the irregular Voronoi polygons cannot be approximated as beams. Hence, we have to use the vertices of the Voronoi polygons to compute the beam border by approximating the Voronoi polygons to ellipses.

D. ELLIPTIC APPROXIMATION

Considering the mathematical tractability and topological packing, we can approximate the beam footprint to either a circle or an ellipse. However, a circular approximation of the Voronoi polygons will overlap beams and will cause inter-beam interferences. Hence, to reduce overlapping of beams and to have full coverage, we approximate the Cartesian coordinates of the boundaries of the Voronoi polygon vertices into ellipses to represent them as beam footprint.

Accordingly, we divide (7) on both sides by a and move x^2 to the right-hand side as,

$$2bxy + cy^2 + 2dx + 2fy + g = -x^2, \tag{15}$$

and then define M and p as,

$$M = \begin{bmatrix} 2x_1y_1 & y_1^2 & 2x_1 & 2y_1 & 1 \\ 2x_2y_2 & y_2^2 & 2x_2 & 2y_2 & 1 \\ \vdots & \vdots & \vdots & \vdots & \vdots \\ 2x_sy_s & y_s^2 & 2x_s & 2y_s & 1 \end{bmatrix}, \tag{16a}$$

$$p = \begin{bmatrix} b & c & d & f & g \end{bmatrix}^T, \tag{16b}$$

such that we can represent (15) as $M \times p = b'$. To solve for p, we use an estimation technique in (15) and represent it as $M \times p = b'$. As we know the elements in M which are the vertices of the covex Voronoi polygon, we find the pseudo inverse (M^+) matrix of M. Then we assume $b' = -x^2$ and solve for p as $p = M^+ \times b'$. Hence, by solving for p, we will have best parameters for a, b, c, d, f, g in the Least Square sense.

The parameters a, b, c, d, f, g are now used to obtain center, semi-major axis, semi-minor axis and the phase angle of the ellipse [42]. The centre of the ellipse is obtained using,

$$x_0 = \frac{cd - bf}{b^2 - ac}, \tag{17a}$$

$$y_0 = \frac{af - bd}{b^2 - ac}. \tag{17b}$$

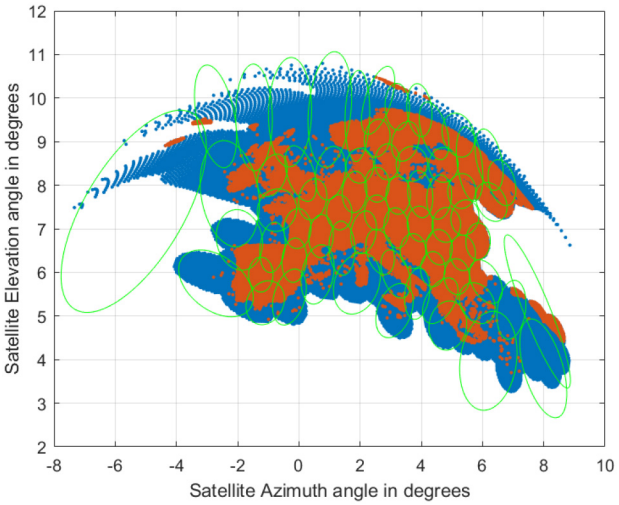

FIGURE 8. Beam Footprint as ellipses (shown using green) over Europe using 71 Adaptive Beams in satellite angular domain. Sampled coverage area is shown in blue and the user positions are shown in red.

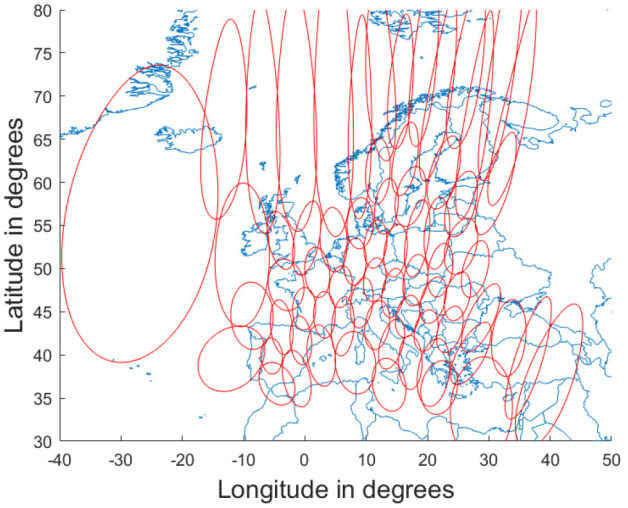

FIGURE 9. Projection of 71 ellipses (shown in red) on the surface of the Earth over Europe.

The semi-major axis and the semi-minor axis are derived using,

$$axis_1 = \sqrt{\frac{2\left(af^2 + cd^2 + gb^2 - 2bdf - acg\right)}{\left(b^2 - ac\right)\left(\sqrt{(a-c)^2 + 4b^2}\right) - (a+c)}}, \quad (18a)$$

$$axis_2 = \sqrt{\frac{2\left(af^2 + cd^2 + gb^2 - 2bdf - acg\right)}{\left(b^2 - ac\right)\left(-\sqrt{(a-c)^2 + 4b^2}\right) - (a+c)}}, \quad (18b)$$

where the bigger axis among $axis_1$ and $axis_2$ is the semi-major axis and smaller axis among $axis_1$ and $axis_2$ is the semi-minor axis.

The angle of rotation of the ellipse that best fits the Voronoi convex polygon is derived using,

$$\varphi = \begin{cases} 0, & \text{for } b = 0; a < c \\ \frac{1}{2}, & \text{for } b = 0; a > c \\ \frac{1}{2}\cot^{-1}\frac{a-c}{2b}, & \text{for } b \neq 0; a < c \\ \frac{\pi}{2} + \frac{1}{2}\cot^{-1}\frac{a-c}{2b}, & \text{for } b \neq 0; a > c. \end{cases} \quad (19)$$

The approximated ellipses from the Voronoi polygon in the satellite angular domain is shown in Figure 8. The centres of the ellipses ($\boldsymbol{c}_k$) will represent the proposed adaptive beams centres/positions. The semi-major and semi-minor axis of the approximated ellipses ($\delta\theta_k$, $\delta\phi_k$) defines the boundary of the proposed adaptive beams. The angle of rotation of approximated ellipses (φ_k) represents the orientation of the proposed adaptive beams.

The approximated ellipses on the satellite antenna domain projected on the surface of the Earth are shown in Figure 9. The domain conversion of the ellipses from the satellite antenna domain to the surface of the Earth is the reverse operation of what is discussed in IV-A. It can be noticed that, on the surface of the Earth, the ellipse are distorted due to the curvature of the Earth.

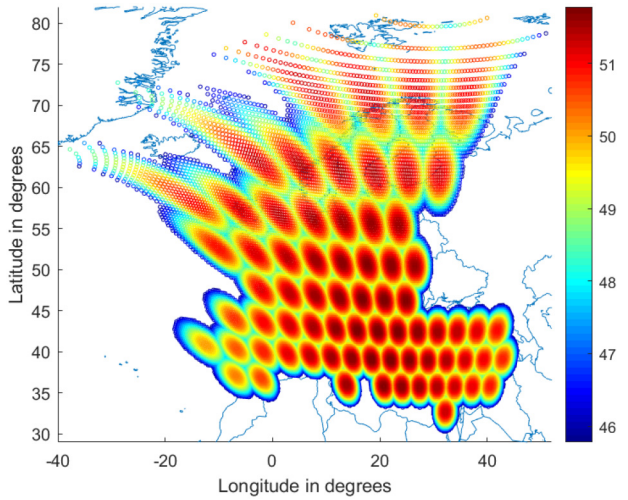

FIGURE 10. Antenna pattern of FMPF plan where the colour bar represents Antenna gain values on the surface of the Earth.

E. ANTENNA GAIN CALCULATION

In real satellite antenna pattern of FMPF benchmark [20]–[22] shown in Figure 10, the antenna gain values distributed across the coverage region is sampled at coverage points on the surface of the Earth. In the satellite angular domain, the coverage points and their corresponding antenna gain values are shown in Figure 11. The proposed AMPF beams are elliptical in the angular domain of the satellite and hence, we approximate the antenna gains of the AMPF antenna pattern using two-dimensional Gaussian elliptical function. The antenna gain at any point of the AMPF elliptical beam could be modelled using,

$$f(x,y) = A\exp\Big(-\Big(m_1(x-x_o)^2 + 2m_2(x-x_o)(y-y_o) + m_3(y-y_o)^2\Big)\Big), \quad (20)$$

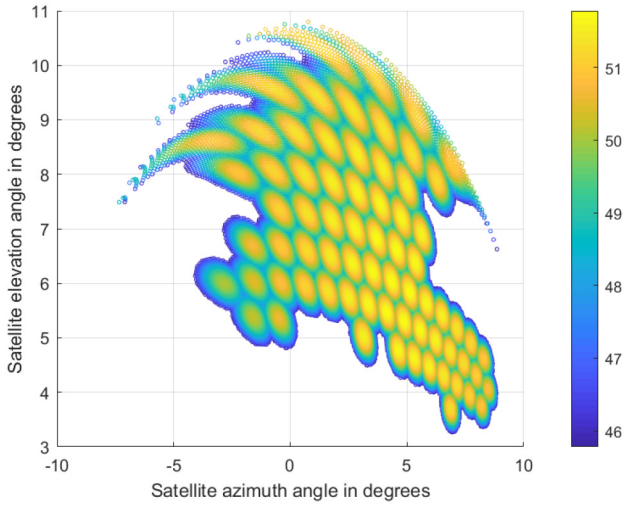

FIGURE 11. Antenna pattern of FMPF plan where the colour bar represents Antenna gain values on the satellite angular domain.

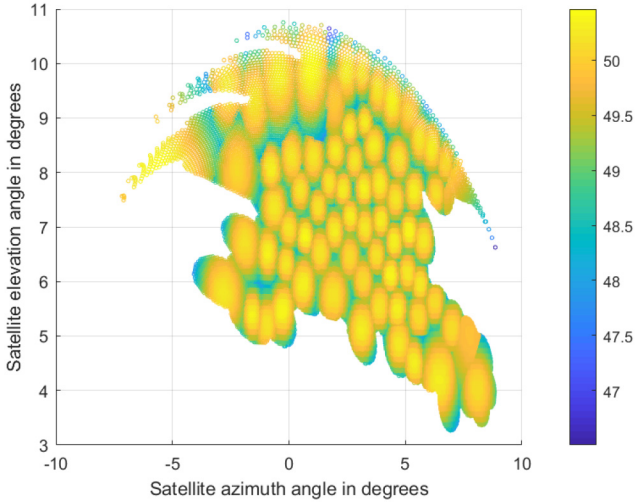

FIGURE 12. Antenna pattern of proposed AMPF plan where the colour bar represents Antenna gain values on the satellite angular domain.

where the matrix $\begin{bmatrix} m_1 & m_2 \\ m_2 & m_3 \end{bmatrix}$ is positive-definite matrix [43].

As the proposed elliptical AMPF beams are fitted with the two-dimensional Gaussian elliptical function, the semi-major axis of the ellipse ($\delta\theta$) is fitted with σ_X of the Gaussian function and semi-minor axis of the ellipse ($\delta\phi$) of the ellipse is fitted with σ_Y of the Gaussian function. The coefficient A is the amplitude of boresight point or maximum antenna gain. The centre of the Gaussian function (intersection point of σ_x and σ_y) is the centre (x_0, y_0) of the ellipse. The values of $m1, m2$ and $m3$ are defined using,

$$m_1 = \frac{\cos^2\varphi}{2\sigma_X^2} + \frac{\sin^2\varphi}{2\sigma_Y^2}, \tag{21a}$$

$$m_2 = -\frac{\sin 2\varphi}{4\sigma_X^2} + \frac{\sin 2\varphi}{4\sigma_Y^2}, \tag{21b}$$

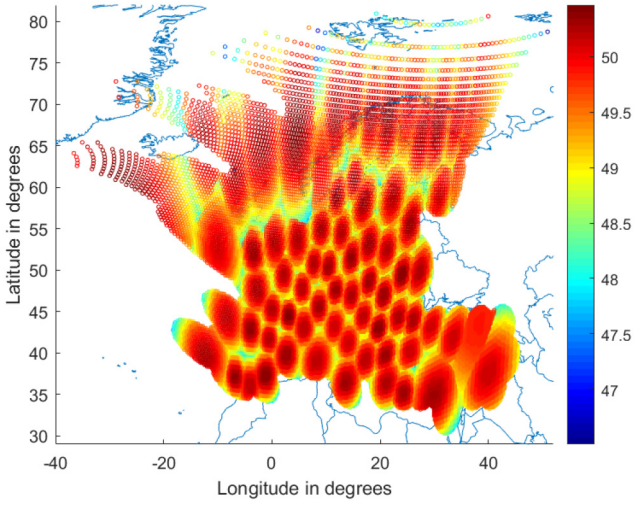

FIGURE 13. Antenna pattern of proposed AMPF plan where the colour bar represents Antenna gain values on the surface of the Earth.

$$m_3 = \frac{\sin^2\varphi}{2\sigma_X^2} + \frac{\cos^2\varphi}{2\sigma_Y^2}. \tag{21c}$$

For a fair comparison between the proposed AMPF pattern and the benchmark FMPF pattern, Power Flux Density (PFD) measured in Watts per square meters W/m^2 of the proposed FMPF beams should be similar to the PFD of benchmark FMPF beams. Also, the total transmission power of the proposed AMPF scheme should be approximately equal to the FMPF benchmark plan. We achieve this by optimizing antenna gains of the AMPF beams at the sampled coverage points on the surface of the Earth. Accordingly, we first integrate the power at sampled coverage points of every beam in the FMPF benchmark pattern and then normalize the power of every beam in the AMPF beams, such that the power of every proposed AMFP beam is equal to the average power of the FMPF benchmark beams.

After fitting the two-dimensional Gaussian function upon the proposed elliptical AMPD beams and optimizing its PFD to the average PFD of the FMPD beams, we can obtain the antenna gain value at any sampled coverage points on the surface of the Earth. In the satellite angular domain, the sampled coverage points and their corresponding antenna gain values of the proposed AMPF antenna pattern are shown in Figure 12. Also, Figure 13 shows the antenna gain values of the proposed AMPF antenna pattern at sampled coverage points on the surface of the Earth. Furthermore, using this antenna gain values, we can determine SNR and the offered throughput for any user at sampled coverage points on the surface of the Earth.

V. SIMULATION AND RESULTS

A. DATA SET MODEL AND LINK BUDGET

The data sets that are employed for simulations are collected from authentic sources to present an accurate traffic model. The simulation parameters and the link budget information

TABLE 2. Simulation parameters.

Satellite longitude	0 degree East (GEO)
Total Number of Beams, N˙B	71
Uplink C/N	18.4 dB
Power per beam	13 W
Number of beams per TWTA	1
Number of carriers per TWTA	1
Number of carriers per beam	1
Carrier Frequency	19.96 GHz
Carrier Bandwidth	216 MHz
Useful Bandwidth	216 MHz
Roll off	0.05
Symbol Rate	205 Msps
OBO	3.8 dB
NPR	20 dB
Payload degradations	2 dB
Free space distance	37000 km
Wavelength	0.015182186
Free space path loss	209.7215455 dB
Rain Fade (99.5%)	2 dB
Other losses	2 dB

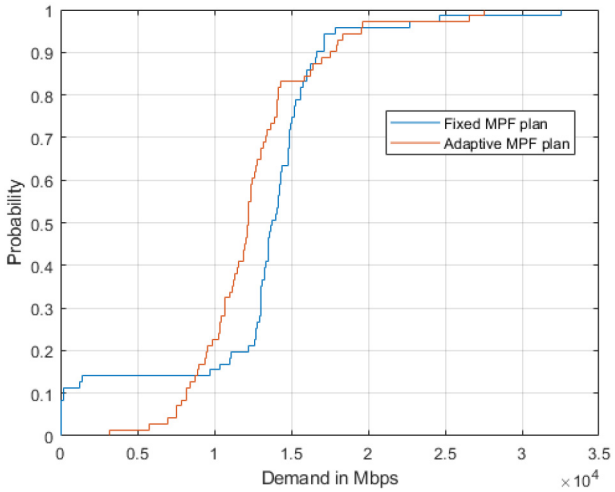

FIGURE 14. Empirical Cumulative Distribution Function (CDF) showing the system demand distribution across all the beams.

considered for the proposed AMPF plan is summarized in the Table 2.

Also, we consider a total number of $N = 60617$ users distributed across the coverage area of $K = 71$ beams whose location and demand is extracted using the SnT traffic simulator [32]. We denote the traffic demand of the generic user n, in *bps*, as d_n using [32]. The SnT traffic emulator [32] models the broadband traffic demand distribution over Europe including users from Population distribution for broadband Fixed Satellite Services (FSS), aeronautical satellite communications, and vessel distribution for maritime services. The number of flights corresponding to their coverage area is considered, where the aeronautical data is deduced from anonymized and unfiltered flight-tracking source [44]. The container ship distribution for maritime is included and evaluated by dataset obtained from vessel tracking Web site (VesselFinder) which includes ship positions and marine traffic detected by global AIS network [45]. The Population data is used to generate the traffic distribution for broadband Fixed satellite services (FSS) terminals and has been extracted from the NASA Socioeconomic Data and Applications Center (SEDAC) population database [46]. These large-scale and fine-grained datasets guarantee the reliability and the consistency of our traffic pattern analysis and modelling.

B. NUMERICAL RESULTS

1) DEMAND DISTRIBUTION

The beam demand D_k (in bps) of a beam k is the summation of traffic demand of all the users belonging to the beam k and is expressed as,

$$D_k = \sum_{n \in \mathcal{T}^k} d_n, \tag{22}$$

and the total system demand (in bps) is the summation of all the beam demands in the Multi-beam HTS system and is expressed using,

$$D_{sys} = \sum_{k=1}^{K} D_k, \tag{23}$$

where $n = 1, 2, \ldots, N$ are the number of users, $k = 1, 2, \ldots, K$ are the number of beams, d_n (in bps) is traffic demand of the user n. $\mathcal{T}^k$ is the set containing all the users that belong to beam k.

The main objective of this work is to distribute D_{sys} evenly among the K beams. To verify this, we computed beam demands $D_k \forall k$ for both benchmark FMPF plan and proposed AMPF plan and plotted Empirical Cumulative Distribution Function (CDF) as shown in Figure 14. In AMPF plan, probability of having any beams with zero demand is zero whereas in FMPF plan, probability of having any beams with zero demand is around 0.1. Also, the probability of having beams with lower demand (< 8 Gbps) is higher in FMPF plan than AMPF plan and the probability of having beams with higher demand (> 26 Gbps) is higher in FMPF plan than AMPF plan.

Hence, the proposed AMPF plan has clearly reduced beam demand for beams with high demands and distributed it to the beams with relatively lower demand. Furthermore, it ensures that no beam is planned with zero demand. Whereas, in the benchmark FMPF plan, the total system demand is more unequally distributed. Also, some beams are having zero beam demand that has to be met. This is majorly because in rigid fixed plan, the geographical broadband user locations and their traffic demand is ignored and hence some beams are pointed to geographic locations on the Earth where no broadband users are present. Alternatively, the proposed AMPF plan distributes system demand more evenly and ensures that beams are always assigned with an adequate beam demand that have to be met.

The Jain's Fairness Index ($\mathfrak{J}$) [47] is a well-known fairness metric, which in this context measures how evenly the

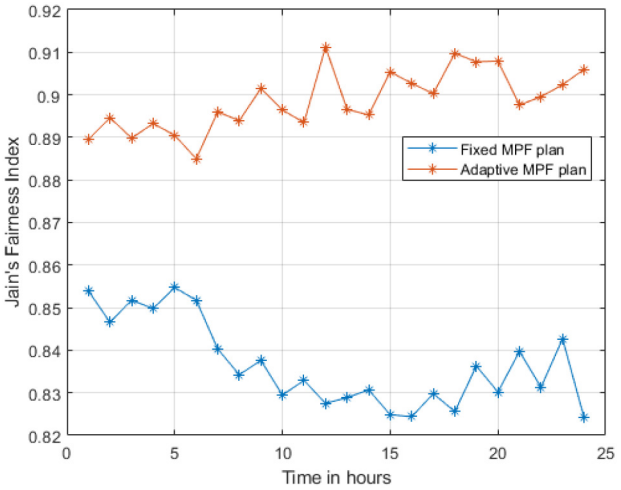

FIGURE 15. Jain's Fairness Index ($\mathfrak{J}$) at different time stamps of a day.

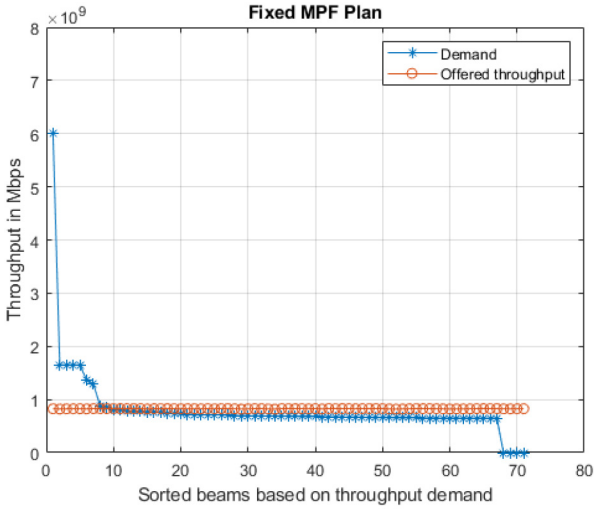

FIGURE 16. Throughput demand requested and offered throughput to any user in the benchmark FMPF plan beams.

demand is distributed across all the beams. Specifically, if D_k is the summation of demand of all the users in beam k, the Jain's fairness index is defined as,

$$\mathfrak{J} = \frac{\left(\sum_{k=1}^{K} D_k\right)^2}{K \sum_{k=1}^{K} D_k^2}, \tag{24}$$

and ranges between $\frac{1}{K}$ and 1, where $\frac{1}{K}$ signifies that the system is least fair and 1 signifies that the system is most fair. The Jain's fairness index is computed for both benchmark FMPF plan and proposed AMPF plan at different time stamps of a day and is shown in Figure 15. It is evident that the proposed AMPF plan performs better with value much closer to 1 in comparison to the benchmark FMPF plan.

2) DEMAND REQUESTED AND OFFERED THROUGHPUT

The throughput demand $d_{\forall n,k}$ requested by any user n in beam k is defined using,

$$d_{\forall n,k} = \frac{1}{|\mathcal{T}^k|} \sum_{n \in \mathcal{T}^k} d_n, \tag{25}$$

where $\mathcal{T}^k$ is the set containing all the users that belong to beam k and d_n (in bps) is traffic demand of the user n. The cardinality of a set $\mathcal{T}^k$ is denoted $|\mathcal{T}^k|$.

In FMPF benchmark antenna pattern, the antenna gain values distributed across the coverage region is sampled at coverage points on the surface of the Earth. We define such sampled coverage points as $p = 1, 2, \ldots, P$, where P is the total number of sampled coverage points under the entire coverage region of the satellite in FMPF plan. We define Signal-to-Noise ratio (SNR) as SNR_p^F at any sampled coverage point p in the FMPF plan. Also, as the granularity of the sampled coverage point is fine, we approximate the SNR experienced by any user n to the SNR of the closest sampled coverage point p.

The offered throughput ($R^F_{\forall n,k}$) to any user in a beam k can be defined using,

$$R^F_{(\forall n,k)} = \frac{1}{|P_k^F|} \left(\sum_{p \in P_k^F} B \log_2\left(1 + SNR_p^F\right) \right), \tag{26}$$

where B is the system bandwidth and the set P_k^F is the set containing all the sampled coverage points that belong to beam k. The cardinality of a set P_k^F is denoted $|P_k^F|$. For the benchmark FMPF plan, the SNR at a sampled coverage point (p) is computed using the FMPF benchmark antenna pattern from the dataset provided by [32]. Also, we use four colour frequency reuse scheme which makes inter-beam interference negligible.

To ensure a fair comparison between the FMPF plan and the proposed AMPF plan, we consider computing the offered throughput of proposed AMPF plan at previously defined sampled coverage points ($p = 1, 2, \ldots, P$) of FMPF plan. Accordingly, in the proposed AMPF plan, we define SNR at any sampled coverage point p as SNR_p^A. The offered throughput ($R^A_{(\forall n,k)}$) to any user n in a beam k can be defined using,

$$R^A_{(\forall n,k)} = \frac{1}{|P_k^A|} \left(\sum_{p \in P_k^A} B \log_2\left(1 + SNR_p^A\right) \right), \tag{27}$$

where SNR at sampled coverage points (p) are computed using antenna gain values at sampled coverage points obtained by fitting the two-dimensional Gaussian function as discussed in IV-E. The set P_k^A is the set containing all the sampled coverage points that belong to beam k. The cardinality of a set P_k^A is denoted $|P_k^A|$.

Figure 16 shows the throughput demand requested by any user in the benchmark FMPF plan beams. For better visualization the beams are sorted based on the throughput demand

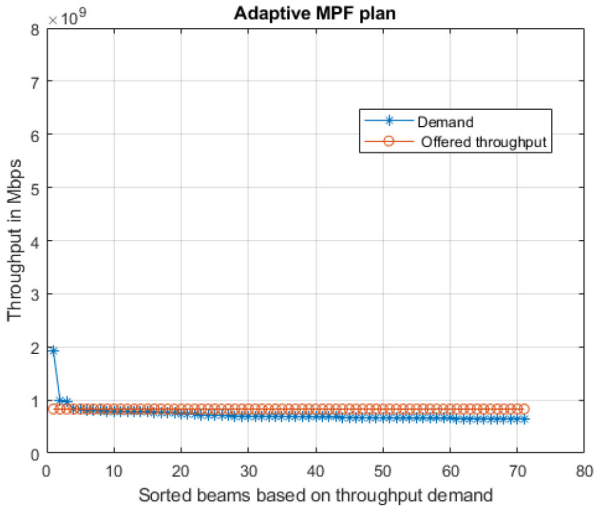

FIGURE 17. Throughput demand requested and offered throughput to any user in the proposed AMPF plan beams.

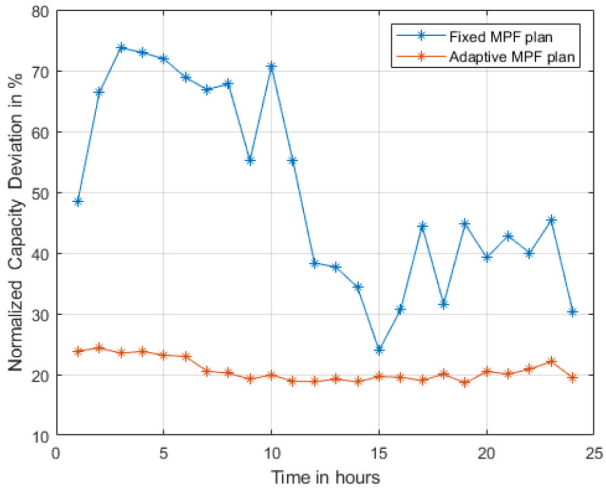

FIGURE 18. Normalized Capacity Deviation (NCD) in percentage at different time stamps of a day.

before plotting. From Figure 16 it is evident that throughput demand requested by any user in beams 1 to 6 are very high. Also, as there are no users from beam 63 to 71, the throughput demand requested by any user is zero. However, the offered throughput to any user in the FMPF beams remains same. Hence, the demand requested by any user in beams 1-6 are not met. Also, the offered throughput to beams 63-71 is unused due to the absence of users.

Figure 17 shows the throughput demand requested by any user in the proposed AMPF plan beams. For better visualization the beams are sorted based on the throughput demand before plotting. From the Figure 17, it is evident that throughput demand requested by any user in all the beams is almost identical. Hence, the offered throughput to any user in the AMPF beams is met in almost all the beams.

3) CAPACITY UNUSED/UNMET

Considering $R_{\forall n,k}$ as the offered throughput and $d_{\forall n,k}$ as throughput demand for any user in beam k, We define a set U_1 that contains all the values of k that satisfies $R_{\forall n,k} > d_{\forall n,k}$ and set U_2 that contains all the values of k that satisfies $d_{\forall n,k} > R_{\forall n,k}$. Then unused capacity and unmet capacity for the whole system can be computed using,

$$C_{unused} = \sum_{k \in U_1} \left(R_{\forall n,k} - d_{\forall n,k}\right), U_1 = \left\{\forall k | R_{\forall n,k} > d_{\forall n,k}\right\}, \tag{28a}$$

$$C_{unmet} = \sum_{k \in U_2} \left(d_{\forall n,k} - R_{\forall n,k}\right), U_2 = \left\{\forall k | d_{\forall n,k} > R_{\forall n,k}\right\}. \tag{28b}$$

The Normalized Capacity Deviation (NCD) in percentage for the benchmark FMPF plan and the proposed AMPF plan system can be computed using,

$$NCD = \frac{(C_{unused} + C_{unmet})}{\sum_{k=1}^{K} d_{\forall n,k}}. \tag{29}$$

The geographic locations of the broadband users and their requested throughput demand changes with time. Hence, Using (28a), (28b) and (29), the NCD for the benchmark FMPF plan and proposed AMPF plan is computed at different time instances of a day. From Figure 18, it is evident that the proposed AMPF plan performs better than the benchmark FMPF plan throughout the day. Furthermore, the Normalized Capacity Deviation of benchmark FMPF plan changes drastically with time. While at 03:00 time stamp, 73% of the capacity is unused/unmet, at 15:00 time stamp, 23% of the capacity is unused/unmet. This clearly shows that the benchmark FMPF plan performs poorly when the geographic locations of the users and their traffic demand is variable. Meanwhile, the Normalized Capacity Deviation of proposed AMPF plan remains relatively same throughout the day and hence will be more suitable for mobile non-uniformly distributed broadband traffic users with variable traffic demand.

The dynamics of the load changes play a vital role in the success of the proposed scheme. Nevertheless, based on the data obtained from [44]–[46], the traffic demand varies slowly compared to the time needed for beam adaptation. Accordingly, in our simulations, we introduced adaptability based on the load changes once every hour. However, this adaptation could be made more often or even less often depending upon the changes in the traffic demand. Another approach is to trigger the proposed AMPF planning whenever a threshold change is noticed. Nevertheless, the complexity of the proposed AMPF scheme concerning demand dynamics strongly depends on the frequency of adapting the plan. Hence, such decisions are purely based on satellite operators operational decisions on how often they would want to adopt and hence was beyond the scope of this study.

VI. CONCLUSION

In this work, we present a comprehensive overview of the beam pattern and footprint planning in a High Throughput

Multi-beam Satellite communication systems. Also, we include a detailed analysis of the benchmark Fixed Multi-beam Pattern and Footprint (FMPF) plan and its drawbacks, especially for non-uniform and mobile broadband user distribution with heterogeneous traffic demand. As the FMPF plan fails to distribute the total system demand across all the beams evenly, we propose an Adaptive Multi-beam Pattern and Footprint (AMPF) plan as a relatively better solution. A step by step procedure involved in AMPF plan such as satellite angular domain transformation, weighted k-means clustering of users, Voronoi Tessellation for full coverage region, Ellipse approximation of Voronoi polygon has been discussed in detail.

The simulations conducted using reliable data-sets clearly show a better performance of the proposed AMPF plan in comparison to the benchmark FMPF plan. The proposed AMPF plan distributes the total system demand more evenly and also guarantees coverage region similar to FMPF plan. Also by choosing proposed AMPF plan over the fixed rigid plan, the unused/unmet system capacity reduces.

REFERENCES

[1] A. Kyrgiazos, B. Evans, P. Thompson, P. Mathiopoulos, and S. Papaharalabos, "A terabit/second satellite system for European broadband access: A feasibility study," *Int. J. Satell. Commun. Netw.*, vol. 32, no. 2, pp. 63–92, 2014.

[2] K. S. Rao, M. Q. Tang, and C. Hsu, "Multiple beam antenna technology for satellite communications payloads," *Appl. Comput. Electromagn. Soc. J.*, vol. 21, no. 3, pp. 353–363, Nov. 2006.

[3] G. Maral, B. Michel, and S Zhili, *Satellite Communications Systems: Systems, Techniques and Technology*, 6th ed. Hoboken, NJ, USA: Wiley, 2020.

[4] D. Digdarsini, M. Kumar, and T. V. S. Ram, "Design & hardware realization of FPGA based digital beam forming system," in *Proc. 3rd Int. Conf. Signal Process. Integr. Netw. (SPIN)*, 2016, pp. 275–278, doi: 10.1109/SPIN.2016.7566703.

[5] K. S. Rao, M. Cuchanski, and M. Q. Tang, "Multiple beam antenna concepts for satellite communications," in *Proc. Symp. Antenna Technol. Appl. Electromagn.*, Ottawa, ON, Canada, 1994, pp. 289–292.

[6] S. K. Rao, "Advanced antenna technologies for satellite communications payloads," *IEEE Trans. Antennas Propag.*, vol. 63, no. 4, pp. 1205–1217, Apr. 2015, doi: 10.1109/TAP.2015.2391283.

[7] M. Schneider, H. Christian, and W. Helmut, "Antennas for multiple spot beam satellites," *CEAS Space J.*, vol. 2, no. 1, pp. 59–66, 2011.

[8] C. Balanis, *Antenna Theory: Analysis and Design*, 4th ed. Hoboken, NJ, USA: Wiley-Intersci., 2016.

[9] K. Y. Jo, *Satellite Communications Network Design and Analysis* (Artech House Antennas and Propagation Library). Norwood, MA, USA: Artech House, 2011.

[10] Y. Su, Y. Liu, Y. Zhou, J. Yuan, H. Cao, and J. Shi, "Broadband LEO satellite communications: Architectures and key technologies," *IEEE Wireless Commun.*, vol. 26, no. 2, pp. 55–61, Apr. 2019, doi: 10.1109/MWC.2019.1800299.

[11] M. Takahashi, Y. Kawamoto, N. Kato, A. Miura, and M. Toyoshima, "Adaptive power resource allocation with multi-beam directivity control in high-throughput satellite communication systems," *IEEE Wireless Commun. Lett.*, vol. 8, no. 4, pp. 1248–1251, Aug. 2019, doi: 10.1109/LWC.2019.2912753.

[12] S. Tani, K. Motoyoshi, H. Sano, A. Okamura, H. Nishiyama, and N. Kato, "An adaptive beam control technique for Q band satellite to maximize diversity gain and mitigate interference to terrestrial networks," *IEEE Trans. Emerg. Topics Comput.*, vol. 7, no. 1, pp. 115–122, Jan.–Mar. 2019, doi: 10.1109/TETC.2016.2606107.

[13] S. Kisseleff, M. R. B. Shankar, D. Spano, and J. D. Gayrard, "A new optimization tool for mega-constellation design and its application to trunking systems," in *Proc. 37th Int. Commun. Satell. Syst. Conf. (ICSSC)*, Oct. 2019, pp. 5–8.

[14] M. Takahashi, Y. Kawamoto, N. Kato, A. Miura, and M. Toyoshima, "Adaptive multi-beam arrangement for improving throughput in an HTS communication system," in *Proc. IEEE Int. Conf. Commun. (ICC)*, Dublin, Ireland, 2020, pp. 1–6, doi: 10.1109/ICC40277.2020.9148622.

[15] C. A. Siocos, "Broadcasting-satellite coverage-geometrical considerations," *IEEE Trans. Broadcast.*, vol. BC-19, no. 4, pp. 84–87, Dec. 1973, doi: 10.1109/TBC.1973.266116.

[16] D. Christopoulos, S. Chatzinotas, G. Zheng, J. Grotz, and B. Ottersten, "Linear and nonlinear techniques for multibeam joint processing in satellite communications," *EURASIP J. Wireless Commun. Netw.*, vol. 2012, no. 1, 2012, Art. no. 162.

[17] M. A. Diaz, N. Courville, C. Mosquera, G. Liva, and G. E. Corazza, "Non-linear interference mitigation for broadband multimedia satellite systems," in *Proc. Int. Workshop Satell. Space Commun.*, 2007, pp. 61–65, doi: 10.1109/IWSSC.2007.4409391.

[18] L. Cottatellucci, M. Debbah, G. Gallinaro, R. Mueller, M. Neri, R. Rinaldo, "Interference mitigation techniques for broadband satellite systems," in *Proc. 24th AIAA Int. Commun. Satell. Syst. Conf. (ICSSC).*, San Diego, CA, USA, Jun. 2006, pp. 3–4.

[19] *FlexPreDem—Demonstrator of Precoding Techniques for Flexible Broadband Systems, Activity Code: 3C.014*. Accessed: Dec. 20, 2020. [Online]. Available: https://artes.esa.int/projects/flexpredem

[20] G. Taricco and A. Ginesi, "Precoding for flexible high throughput satellites: Hot-spot scenario," *IEEE Trans. Broadcast.*, vol. 65, no. 1, pp. 65–72, Mar. 2019.

[21] J. Duncan, J. Krivochiza, S. Andrenacci, S. Chatzinotas, and B. Ottersten, "Hardware demonstration of precoded communications in multibeam UHTS systems," in *Proc. 36th Int. Commun. Satell. Syst. Conf. (ICSSC)*, Niagara Falls, ON, Canada, 2018, pp. 1–5.

[22] M. G. Kibria, E. Lagunas, N. Maturo, D. Spano and S. Chatzinotas, "Precoded cluster hopping in multibeam high throughput satellite systems," in *Proc. IEEE Global Commun. Conf. (GLOBECOM)*, Waikoloa, HI, USA, 2019, pp. 1–6.

[23] C. Wu, K. Ece, and E. Horvitz, "Clustering for set partitioning: A case study in carpooling," in *Proc. Workshop Optim. Mach. Learn. (OPT) NIPS*, May 2015, pp. 1–7. [Online]. Available: https://www.microsoft.com/en-us/research/publication/clustering-set - partitioning-case-study-carpooling/

[24] R. M. Karp, "Reducibility among combinatorial problems," in *Complexity of Computer Computations* (IBM Research Symposia Series), R. E. Miller, J. W. Thatcher, J. D. Bohlinger, Eds. Boston, MA, USA: Springer, doi: 10.1007/978-1-4684-2001-2_9.

[25] M. W. Padberg, "On the facial structure of set packing polyhedra," *Math. Program.*, vol. 5, pp. 199–215, Dec. 1973, doi: 10.1007/BF01580121.

[26] X. Gandibleux, X. Delorme, and V. T'Kindt, "An ant colony optimisation algorithm for the set packing problem," in *Ant Colony Optimization and Swarm Intelligence*. Heidelberg, Germany: Springer, 2004, pp. 49–60.

[27] L. Kaufman and P. J. Rousseeuw, *Finding Groups in Data: An Introduction to Cluster Analysis*. Hoboken, NJ, USA: Wiley-Intersci., 2005.

[28] P. Awasthi, A. S. Bandeira, M. Charikar, R. Krishnaswamy, S. Villar, and R. Ward, "Relax, no need to round: Integrality of clustering formulations," 2015. [Online]. Available: arXiv:1408.4045.

[29] W. V. Parker and J. E. Pryor, "Polygons of greatest area inscribed in an ellipse," *Amer. Math. Monthly*, vol. 51, no. 4, pp. 205–209, 1944.

[30] T. Wigren, "A polygon to ellipse transformation enabling fingerprinting and emergency localization in GSM," *IEEE Trans. Veh. Technol.*, vol. 60, no. 4, pp. 1971–1976, May 2011, doi: 10.1109/TVT.2011.2120637.

[31] D. Eberly. *Geometric Tools*. Accessed: Dec. 20, 2020. [Online]. Available: https://www.geometrictools.com/Documentation/InformationAboutEllipses.pdf

[32] H. Al-Hraishawi, E. Lagunas, and S. Chatzinotas, "Traffic simulator for broadband satellite communication systems," in *Proc. ASMS/SPSC Virtual Conf.*, Oct. 2020, pp. 1–8.

[33] E. W. Weisstein. *MathWorld-A Wolfram Web Resource: Spherical Coordinates*. Accessed: Dec. 20, 2020. [Online]. Available: https://mathworld.wolfram.com/SphericalCoordinates.html

[34] T. Iguchi, D. G. Mixon, J. Peterson, and S. Villar, "On the tightness of an SDP relaxation of k-means," May 2015. [Online]. Available: arXiv:1505.04778.

[35] Q. Du, V. Faber, and M. Gunzburger, "Centroidal voronoi tessellations: Applications and algorithms," *Soc. Indus. Appl. Math.*, vol. 41, no.4, pp. 637–676, 1999.
[36] U. Fayyad and R. Uthurusamy, "Data mining and knowledge discovery in databases," *Commun. ACM*, vol. 39, no. 11, pp. 24–26, 1996.
[37] D. Xu and Y. Tian, "A comprehensive survey of clustering algorithms," *Ann. Data Sci.*, vol. 2, no. 2, pp. 165–193, 2015, doi: 10.1007/s40745-015-0040-1.
[38] S. Lloyd, "Least squares quantization in PCM," *IEEE Trans. Inf. Theory*, vol. 28, no. 2, pp. 129–137, Mar. 1982, doi: 10.1109/TIT.1982.1056489.
[39] D. Arthur and S. Vassilvitskii, "K-Means++: The advantages of careful seeding," in *Proc. 18th Annu. ACM-SIAM Symp. Discr. Algorithms*, 2007, pp. 1027–1035.
[40] R. Apu and M. Gavrilova, *Generalized Voronoi Diagram: A Geometry-Based Approach to Computational Intelligence*, vol. 158. Berlin, Germany: Springer, 2009, pp. 109–129.
[41] D. Reem, "An algorithm for computing voronoi diagrams of general generators in general normed spaces," in *Proc. 6th Int. Symp. Voronoi Diagrams*, 2009, pp. 144–152, doi: 10.1109/ISVD.2009.23.
[42] E. W. Weisstein. *MathWorld-A Wolfram Web Resource: Ellipse*. Accessed: Dec. 20, 2020. [Online]. Available: https://mathworld.wolfram.com/Ellipse.html
[43] N. Nawri. *Berechnung von Kovarianzellipsen, Web Resource*. Accessed: Dec. 20, 2020. [Online]. Available: ttp://imkbemu.physik.uni-karlsruhe.de/ēisatlas/ covariance_ellipses.pdf
[44] (Nov. 2020). *ADS-B Exchange—World's Largest Source of Unfiltered Flight Data*. [Online]. Available: https://www.adsbexchange.com/data/
[45] (Nov. 2020). *AIS Ship Tracking of Marine Traffic*. [Online]. Available: https://www.vesselfinder.com/
[46] (Nov. 2020). *NASA, Socioeconomic Data and Applications Center (SEDAC)*. [Online]. Available: http://sedac.ciesin.columbia.edu
[47] R. Jain, D. Chiu, and W. Hawe, "A quantitative measure of fairness and discrimination for resource allocation in shared systems," Digit. Equip. Corp., Maynard, MA, USA, Rep. DEC-TR-301, 1984.

PUNEETH JUBBA HONNAIAH (Graduate Student Member, IEEE) received the Bachelor of Engineering degree in electronics and communication engineering from Visvesvaraya Technological University, India, in 2012, and the Master of Science degree in electronics and communication engineering from Hochschule Bremen–City University of Applied Sciences, Germany, in 2017. He is currently pursuing the Ph.D. degree with the Signal Processing and Satellite Communications Group, SIGCOM, Interdisciplinary Centre for Security, Reliability and Trust, University of Luxembourg, where he is a Doctoral Researcher. He has worked several years in the telecom industry and has expertise in satellite communication, GSM, LTE, and 5G technologies.

NICOLA MATURO (Member, IEEE) received the M.S. degree (*cum laude*) in electronic engineering and the Ph.D. degree in telecommunication engineering from the Polytechnic University of Marche, Ancona, Italy, in 2012 and 2015, respectively. From January 2016 to July 2017, he was a Postdoctoral Researcher with the Department of Information Engineering, Polytechnic University of Marche, where he worked on error correcting coding techniques under some ESA research projects. From November 2015 to May 2016, he was a Consultant for Deimos Engenharia, Lisbon, Portugal, working on spectral estimation algorithms and anti-jamming techniques. Since August 2017, he has been a Research Associate with the University of Luxembourg. His research activity is mainly focused on the development and implementation of advanced techniques for satellite communication. He has been a member the CCSDS Coding and Synchronization Working Group since 2015.

SYMEON CHATZINOTAS (Senior Member, IEEE) received the M.Eng. degree in telecommunications from the Aristotle University of Thessaloniki, Thessaloniki, Greece, in 2003, and the M.Sc. and Ph.D. degrees in electronic engineering from the University of Surrey, Surrey, U.K., in 2006 and 2009, respectively. He is currently a Full Professor/Chief Scientist I and the Co-Head of the SIGCOM Research Group, SnT, University of Luxembourg. He has been a Visiting Professor with the University of Parma, Italy, and he was involved in numerous Research and Development projects for the National Center for Scientific Research Demokritos, the Center of Research and Technology Hellas and the Center of Communication Systems Research, University of Surrey. He has (co) authored more than 400 technical papers in refereed international journals, conferences and scientific books. He was a co-recipient of the 2014 IEEE Distinguished Contributions to Satellite Communications Award, the CROWNCOM 2015 Best Paper Award and the 2018 EURASIC JWCN Best Paper Award. He is currently in the editorial board of the IEEE OPEN JOURNAL OF VEHICULAR TECHNOLOGY and the *International Journal of Satellite Communications and Networking*.

STEVEN KISSELEFF (Member, IEEE) received the M.Sc. degree in information technology from the Technical University of Kaiserslautern, Germany, and the Ph.D. degree in electrical engineering from the Friedrich-Alexander University of Erlangen–Nurnberg, Germany, in 2011 and 2017, respectively, where he was Research and Teaching Assistant with the Institute for Digital Communications from October 2011 to July 2018. From November 2012 to March 2013, he was a Visiting Researcher with the State University of New York at Buffalo, USA, and the Broadband Wireless Networking Lab, Georgia Institute of Technology, Atlanta, USA. In 2018, he joined the Interdisciplinary Centre for Security, Reliability and Trust (SnT), University of Luxembourg, as a Research Associate. His research interests lie in the area of digital communications, Internet-of-Things, and satellite communication.

JENS KRAUSE was born in Werdohl, Germany, in 1963. He received the Dipl.-Ing. and Ph.D. degrees in electrical engineering from University of Karlsruhe, Germany, in 1987 and 1993, respectively. He has held a scientific employee position with University of Karlsruhe from 1988 to 1993. From 1994 to 1996, he has been an R&D Engineer with the Cable TV Department, Richard Hirschmann GmbH, Germany. Since 1996, he has been working as a Satellite Operator with SES S.A., Luxembourg, with various positions in systems engineering. He represents SES in standardization organizations, including ETSI and DVB. His research interests include satellite communications in general, modulation and coding, and signal processing for satellite communications.